Molecular Cancer Therapeutics

Vemurafenib Resistance Signature by Proteome Analysis Offers New Strategies and Rational Therapeutic Concepts

Verena Paulitschke[1], Walter Berger[2], Philipp Paulitschke[3], Elisabeth Hofstätter[1], Bernhard Knapp[4], Ruth Dingelmaier-Hovorka[1], Dagmar Födinger[1], Walter Jäger[5], Thomas Szekeres[6], Anastasia Meshcheryakova[7], Andrea Bileck[8], Christine Pirker[2], Hubert Pehamberger[1], Christopher Gerner[8], and Rainer Kunstfeld[1]

Abstract

The FDA-approved BRAF inhibitor vemurafenib achieves outstanding clinical response rates in patients with melanoma, but early resistance is common. Understanding the pathologic mechanisms of drug resistance and identification of effective therapeutic alternatives are key scientific challenges in the melanoma setting. Using proteomic techniques, including shotgun analysis and 2D-gel electrophoresis, we identified a comprehensive signature of the vemurafenib-resistant M24met in comparison with the vemurafenib-sensitive A375 melanoma cell line. The resistant cells were characterized by loss of differentiation, induction of transformation, enhanced expression of the lysosomal compartment, increased potential for metastasis, migration, adherence and $Ca2^{+}$ ion binding, enhanced expression of the MAPK pathway and extracellular matrix proteins, and epithelial–mesenchymal transformation. The main features were verified by shotgun analysis with QEXACTIVE orbitrap MS, electron microscopy, lysosomal staining, Western blotting, and adherence assay in a VM-1 melanoma cell line with acquired vemurafenib resistance. On the basis of the resistance profile, we were able to successfully predict that a novel resveratrol-derived COX-2 inhibitor, M8, would be active against the vemurafenib-resistant but not the vemurafenib-sensitive melanoma cells. Using high-throughput methods for cell line and drug characterization may thus offer a new way to identify key features of vemurafenib resistance, facilitating the design of effective rational therapeutic alternatives. *Mol Cancer Ther; 14(3); 757–68. ©2015 AACR.*

Introduction

During the past 10 years, the incidence of melanoma has increased more rapidly than that of any other cancer type. Up to one fifth of patients develop metastatic disease, which is associated with poor prognosis and a median survival of 7.5 months. Dacarbazine, the mainstay of treatment for metastatic melanoma over the last 30 years, achieves response rates of 22% but does not improve survival (1). After decades of failed attempts to improve treatment outcomes, two new drugs, ipilimumab and vemurafenib (PLX4032), were shown in randomized phase III clinical trials to significantly enhance overall survival (2, 3). Vemurafenib, a novel small-molecule BRAF inhibitor, was approved by the FDA in August 2011 for the treatment of metastatic or inoperable melanoma harboring a BRAF V600E mutation (4).

Mutational activation of BRAF V600E is one of the most prevalent genetic alterations in human melanoma (50% of all melanomas). Clinical responses, including complete remissions, were achieved with vemurafenib in 80% of patients with BRAF V600E-mutated melanomas. However, acquired drug resistance frequently emerged after 2 to 18 months (5). Despite intensive efforts, an understanding of resistance to BRAF inhibitors has yet to be achieved. The plasticity and heterogeneity of melanoma cells could potentially allow multiple adaptive mechanisms [e.g., epithelial–mesenchymal transition (EMT), and differences in proliferation, motility, or stem cell-like characteristics; ref. 6]. Thus, it is unlikely that a single biomarker would serve to indicate drug resistance.

Proteomics facilitates the most comprehensive insight into the pathophysiological conditions derived from protein expression profiles and enables detection of distinct protein signatures of different cells. In a recent feasibility study, we explored the characteristics of cisplatin resistance in melanoma cell lines and confirmed that proteome profiling and bioinformatics can support the understanding of drug resistance mechanisms, with the potential to guide individually tailored therapy (7).

In the present study, we sought to extend our earlier work (7), using high-throughput techniques such as shotgun analysis and

[1]Department of Dermatology, Medical University of Vienna, Vienna, Austria. [2]Institute of Cancer Research and Comprehensive Cancer Center Vienna, Medical University Vienna, Vienna, Austria. [3]Institute of Physics, Center for NanoScience, Ludwig-Maximilians-University, Munich, Germany. [4]Protein Informatics Group, Department of Statistics, University of Oxford, Oxford, United Kingdom. [5]Department of Clinical Pharmacy and Diagnostics, University of Vienna, Vienna, Austria. [6]Department of Medical and Chemical Laboratory Diagnostics, Medical University of Vienna, Vienna, Austria. [7]Institute of Pathophysiology and Allergy Research, Center for Pathophysiology, Infectiology and Immunology, Medical University of Vienna, Vienna, Austria. [8]Institute of Analytical Chemistry, University of Vienna, Vienna, Austria.

Note: Supplementary data for this article are available at Molecular Cancer Therapeutics Online (http://mct.aacrjournals.org/).

Corresponding Author: Rainer Kunstfeld, Division of General Dermatology, Department of Dermatology, Medical University Vienna, Waehringerguertel 18-20, 1090 Vienna, Austria. Phone: 43-1-40400-62620; Fax: 43-1-40400-78500; E-mail: rainer.kunstfeld@meduniwien.ac.at

doi: 10.1158/1535-7163.MCT-14-0701

2D-gel electrophoresis to compare the features of vemurafenib-sensitive with -resistant melanoma cell lines and identify a comprehensive signature of vemurafenib resistance. On the basis of these findings, we aimed to explore whether proteome analysis could be used to predict sensitivity to a rationally chosen agent, based on its mechanism of action.

Materials and Methods

Cell line and chemicals

The A375 melanoma cell line (ATCC) harbors a mutation in BRAFV600E, whereas the metastatic M24met line harbors a mutation in NRAS, a deletion in p16, and amplification in EGFR. Melanoma cells expressing the BRAF mutation are reported to be vemurafenib sensitive, while resistance may be associated with NRAS mutation or activation (8, 9). The M24met cell line was previously found to be resistant to cisplatin, whereas the A375 was sensitive (7). M24met and A375 melanoma cells were described previously (7, 10) and where obtained in 2005.

M24met cells (kindly provided by Dr. R.A. Reisfeld, Department of Immunology, Scripps Research Institute, La Jolla, CA) were grown in RPMI-1640 supplemented with 10% FBS, 2 mmol/L glutamine, and 50 μg/mL gentamycin sulfate. A375 were grown in D-MEM tissue culture medium supplemented with 10% FBS, 2 mmol/L glutamine, and 50 μg/mL gentamycin sulphate as described previously.

We studied these two cell lines to gain an initial understanding of vemurafenib sensitivity and resistance and subsequently attempted to verify these changes in an established melanoma model with acquired vemurafenib resistance.

For this purpose, we used a vemurafenib-sensitive cell line VM-1, which harbors the mutation BRAF V600E (11). VM-1 cells have been established at the Institute of Cancer Research (Vienna, Austria) from a lymph node metastasis (primary tumor: superficial spreading melanoma) from a female patient in 1978 and were obtained by us in 2012. The cell lines were authenticated at the Institute of Cancer Research in all cases by array comparative genomic hybridization (Agilent; 44 k human whole-genome DNA arrays) as published previously (12) and STR fingerprinting during this study in June 2014.

We generated a series of melanoma cell lines with increasing vemurafenib resistance, by exposing a vemurafenib-sensitive cell line VM-1 (V0) to increasing concentrations of the drug: 0.5, 1, and 10 μmol/L. The resultant cell lines were termed V0.5, V1, and V10, respectively: V0 is the sensitive parent cell line.

3,3′,4,4′,5,5′-hexahydroxystilbene (M8) was provided by the Department of Pharmaceutical Chemistry, University of Vienna, Austria, frozen as 50 or 10 mmol/L stock solutions in DMSO (Sigma-Aldrich) and diluted in RPMI as required (13). Vemurafenib, diluted in DMSO, was purchased from Fa. Eubio.

Cell proliferation assay

The CellTiter 96 AQ_{ueous} Non-Radioactive Cell Proliferation Assay (Promega) was used according to manufacturer's guidelines as described previously (10). In brief, cells are plated in 96-well plates (1,500 cells/well). After 24 hours, increasing concentrations of vemurafenib, M8 or a solvent control (DMSO alone) were added. After 48 hours, proliferation is measured at 490 nm with an ELISA plate reader.

FACS analysis

FACS analysis of A375 and M24met melanoma cells was performed as described previously (14).

Lysosomal staining

Lysosomal staining of vemurafenib-sensitive and -resistant cells was performed as described previously (7) using Lysotracker Red DND-99 (Molecular Probes; L7528). Cells were seeded on coverslips, treated with DMSO or vemurafenib for 48 hours, and incubated with Lysotracker Red for 1 hour at 37°C. Images were captured by a Zeiss confocal microscope.

Scanning electron microscopy

Scanning electron microscopy (SEM) with V0, V0.5, V1, and V10 was performed as described previously (15). Critical point drying was applied. The SEM images were taken at a magnification between 500 and 6,000 using a Leo DSM 982 field emission scanning electron microscope at 4 kV.

CytoSelect 48-well cell adhesion assay (ECM array, colorimetric format)

The ECM Array was performed as described previously (7). Vemurafenib-resistant and -sensitive cells were allowed to attach to ECM-coated well plates for 1 hour at 100,000 cells/well. Unbound cells were washed away and the adherent cells stained and quantified calorimetrically.

IHC staining of the primary melanoma cells

M24met and A375 melanoma cells were grown on tissue culture chamber slides (Nalge Nunc) and fixed in 4% formaldehyde then stained with the primary antibodies HMB45, Melan A, S100 (Dako, Corporation), Nestin (IBL), and p75NTR (Sigma), as described previously (13).

Western blot analysis

Cells (A375, M24met, vemurafenib-sensitive, and -resistant melanoma cells) were frozen in liquid nitrogen and lysed with lysis buffer containing phosphatase and protease inhibitors as described previously (10, 16). Membranes were incubated with the following primary antibodies: monoclonal mouse anti-human Vimentin Clone V9 (Dako), N-cadherin, or E-cadherin (Cell Signaling Technology).

Zymography assay

Zymography Assay was performed as described previously (10). The supernatant of V0, V0.5, V1, and V10 was collected. The SDS gel contained gelatine (1 mg/mL), was stained in Coomassie solution for 30 minutes, and stripped with an isopropanol-acetic acid solution (BioTeZ Berlin-Buch GmbH).

Proteome analysis

Proteome analysis was performed as described previously (7, 10).

Subcellular fractionation and 1D PAGE. All fractionation steps were performed on ice. To obtain the cytoplasmic fraction, A375, M24met, V0, and V1 cells were lysed in isotonic lysis buffer (10 mmol/L HEPES/NaOH, pH 7.4, 0.25 mol/L sucrose, 10 mmol/L NaCl, 3 mmol/L MgCl2, 0.5% Triton X-100) supplemented with protease inhibitors (pepstatin, leupeptin, and aprotinin, each at 1

μg/mL; 1 mmol/L PMSF) and mechanical shear stress. In addition, we performed nuclear fractionation of V0 and V1 cells. By centrifugation at 2,300 × *g* and 4°C for 5 minutes, the cytoplasmic proteins were separated from the nuclei and precipitated overnight with ice-cold ethanol at −20°C. After precipitation, proteins were dissolved in sample buffer (7.5 mol/L urea, 1.5 mol/L thiourea, 4% CHAPS, 0.05% SDS, 100 mmol/L DTT); the determination of protein concentration was carried out using a Bradford assay (Bio-Rad). For gaining nuclear proteins, pellets were swelled up for 10 minutes in extraction buffer (500 mmol/L NaCl) and 1:10 diluted with NP-40 buffer for another 15 minutes. To obtain the nuclear fraction, centrifugation at 2,300 g and 4°C for 5 minutes was performed. The extracted proteins were then precipitated overnight with ice-cold ethanol at −20°C. After precipitation, all samples were dissolved in sample buffer (7.5 mol/L urea, 1.5 mol/L thiourea, 4% CHAPS, 0.05% SDS, 100 mmol/L DDT) and the protein concentrations were determined by means of Bradford assay (Bio-Rad Laboratories). MS-sample preparation 20 μg of each sample was loaded on SDS-PAGE. The different protein fractions were loaded separately on 12% polyacrylamid gels. Electrophoresis was performed until complete separation of a prestained molecular marker (Dual Color, Bio-Rad). Proteins in the gels were stained by a MS-compatible silver staining. After fixation with 50% methanol/10% acetic acid, the gels were washed by bi-distilled water and the proteins inside the gel were sensitized with 0.02% Na2S2O3. Gels were then stained with ice-cold 0.1% AgNO3 for 10 minutes, rinsed by bi-distilled water, and subsequently developed with 3% Na2CO3/0.05% formaldehyde. Afterwards, each protein band was cut into eight slices and destained. Upon reduction with DTT (dithiothreitol) and alkylation with IAA (iodoacetamide), the proteins were digested enzymatically overnight at 37°C using trypsin (Roche Diagnostics). The peptides were eluted, dried, and stored at −20°C until LC/MS analysis.

2D-gel electrophoresis. 2D-gel electrophoresis was performed as described previously (17). The cytosolic protein extracts of A375 and M24met cells used as well for shotgun analysis were loaded by passive rehydration of IPG strips pH 5–8, 17 cm at room temperature followed by isoelectric focusing which was performed in a stepwise fashion (1 hour 0–500 V linear; 5 hours 500 V; 5 hours 500–3,500 V linear; 12 hours 3,500 V). Equilibration was performed with 100 mmol/L DTT and 2.5% iodacetamide according to the manufacturer's instructions (Bio-Rad). For SDS-PAGE, the IPG strips were placed on top of 1.5 mm 12% polyacrylamide slab gels and overlaid with 0.5% low-melting agarose. Gels were stained with a 400 nmol/L solution of Ruthenium II tris (bathophenanthroline disulfonate; RuBPS; ref. 18) and scanned with the FluorImager 595 (Amersham Biosciences) at a resolution of 100 μm. The gels were dried and storage phosphor screens (Molecular Dynamics) were exposed at room temperature for 24 hours. Screens were subsequently scanned using the Phosphorimager SI (Molecular Dynamics) at a resolution of 100 μm. Gels were adjusted to a reference gel with the TT900 S2S software (version 2006.0.2389, Nonlinear Dynamics) and evaluated with the Progenesis software PG200 (version 2006, Nonlinear) using the "same spot" algorithm. Spot assignment, background correction, normalization, and statistical calculations (ANOVA) were performed using this software package. For protein identification, peptides were isolated as described above and separated by nanoflow liquid chromatography (1100 Series LC system, Agilent) as described below.

Shotgun analysis using Agilent nanoflow LC. Peptides of the cytoplasmic fraction of A375 and M24met were separated by nano-flow LC using the HPLC-Chip technology from Agilent, equipped with a 40 nL Zorbax 300SB-C18 trapping column and a 75 μm × 150 mm Zorbax 300SB-C18 separation column. For peptide elution, we applied a gradient from 0.2% formic acid and 3% ACN to 0.2% formic acid and 40% ACN over 60 minutes at a flow rate of 400 nL/minute. Peptide identification was accomplished by MS–MS fragmentation analysis with an iontrap mass spectrometer (XCT-Ultra, Agilent) equipped with an orthogonal nanospray ion source. The MS–MS data were interpreted by the Spectrum Mill MS Proteomics Workbench software (Version A.03.03, Agilent) searching against the SwissProt/UniProtKB protein database for human proteins (Version 12/2010 containing 20328 entries). Capillary voltage was set to 1.75 kV, peptides were searched within a m/z range from 400 to 1,400, fragmentation was triggered for the four highest peptide candidates, allowing for three independent fragmentations and using a dynamic exclusion list lasting for 1 minute. Precursor mass deviation was limited to a maximum of 1.5 Da, the product mass tolerance to maximal 0.7 Da and the minimum matched peak intensity (%SPI) to 70%. A peptide was included in the result files when its SpectrumMill score was above. Peptides scoring between 9 and 13 were only included if precursor m/z value, retention time, and MS2 pattern matched to a reference spectrum scoring above. Concerning protein inference, we chose the smallest number of proteins necessary to explain all observed peptides as described for ProteinProphet. Furthermore, only proteins identified with at least two distinct peptides were included. Selection of protein identification was also based on robustness. Only peptide identifications reproduced in at least two different samples were included. The FDR was determined by searching against the corresponding reversed database. Our filtering steps led to peptide identifications with consistently less than 1% apparent identifications when searching against the reversed database compared with the search against the true database, demonstrating high data accuracy.

Identification details for each protein including all identified peptides, sequence coverage, peptide scores, and MS2 spectra are fully accessible via the PRIDE database (http://www.ebi.ac.uk/pride/).

Shotgun analysis using QEXACTIVE orbitrap MS. Peptides of the cytoplasmic and nuclear fraction V0 and V1 were separated using nanoflow UHPLC (Dionex Ultimate 3000) with a 50 cm × 75 μm 2 μm particle size Pepmap100 column (Thermo Fisher Scientific) and a flow rate of 300 nL/minute, using 100% mobile phase A (98.8% H_2O, 1% ACN, 0.2% FA) and a gradient of mobile phase B (80% ACN, 19.8% H_2O, 0.2% FA) from 8% to 40% solvent B within 240 minutes. Peptides are analyzed in positive ionization mode at a resolution of 70,000 (at m/z = 200) in the range from m/z 400 to 1,400 and fragmented using HCD in a QEXACTIVE orbitrap MS (Thermo) in a data-dependent mode upon fragmentation at 30% normalized collision energy (isolation width of Δm/z = 2, 150 ms collection time, fragmention at 30 eV, resolution 17500 at m/z = 200, top 10 method). All samples were analyzed by LC/MS-MS as duplicates. Data were analyzed using Proteome Discoverer 1.4 equipped with Mascot 2.2 and filtered, allowing a maximum of 5 ppm initial mass deviation for precursor ion spectra and 20 ppm for MS/MS spectra, and only peptides with a FDR less than 0.01 (validation based on q-value). The MS-MS data analysis, including peak list-generation and spectrum

identification, was done using the Spectrum Mill MS Proteomics Workbench software (Version A.03.03, Agilent). We allowed for two missed cleavages and searched against the SwissProt/UniProtKB protein database (Version 12/2010 containing 20328 entries) for human proteins, allowing for precursor mass deviation of 1.5 Da, product mass tolerance of 0.7 Da, and a minimum matched peak intensity (% SPI) of 70%. Because of previous chemical modification, carbamidomethylation of cysteines was set as a fixed modification. Oxidation of methionine was the only posttranslational modification considered.

As described in ref. (19), label-free quantitative data analysis was supported by MaxQuant 1.3.0.5 including the Andromeda search engine and the integrated statistical analysis package Perseus (20, 21). Protein identification was achieved searching against the SwissProt Database (version 012013 with 20 264 entries) allowing a mass tolerance of 5 ppm for MS spectra and 20 ppm for MS-MS spectra. Furthermore, search criteria included a maximum of two missed cleavages, a minimum of two peptide identifications per protein, at least one of them unique, and a FDR less than 0.01 for both, peptide identification as well as protein identification. Again carbamidomethylation of cysteine residues was set as a fixed modification and oxidation of methionine residues and N-terminal protein acetylation as variable modifications. Obtained protein identifications were further analyzed using Perseus (version 1.3.0.4), therefore proteins were filtered for reversed sequences and contaminants as well as a minimum of three independent identifications per protein. Significantly up- and downregulated proteins were determined applying a two-sided *t* test with significance level of $P < 0.05$ (permutation-based correction). In addition, hierarchical clustering was achieved using euclidean distance and average linkage clustering of Z-scored expression values as well as 2D Annotation enrichment analysis was performed based on gene ontology cellular compartment, molecular function, and biologic process terms and Kyoto Encyclopedia of Genes and Genomes pathways according to Geiger and colleagues (22).

Results

Interaction of vemurafenib with the kinase domain of BRAF (V600E)

Vemurafenib is a small-molecule BRAF inhibitor active against V600E-mutated melanoma. Three-dimensional modeling of BRAF bound by vemurafenib and non-liganded BRAF (Fig. 1) shows that vemurafenib may hamper E600 from forming a salt bridge with K507.

Characterization of A375 and M24met

The cisplatin-resistant M24met cell line was found to also be resistant to vemurafenib, whereas the cisplatin-sensitive A375 was also sensitive to vemurafenib (Supplementary Table S1).

IHC and FACS analysis revealed that A375 cells exhibited a small rounded cell shape, whereas M24met were characterized by sprouted cells with a larger cytoplasmic compartment. These cells formed tubes, a characteristic feature of endothelial cells (Supplementary Fig. S1A). M24met and A375 expressed the melanoma marker proteins S100, p75 NTR, and nestin, but were negative for the fibroblast cell marker protein CD90, the endothelial marker proteins CD31 and CD34, and the leukocyte marker protein CD45 (Supplementary Fig. S1C and S1D). A375 cells also showed a higher proliferation rate than M24met.

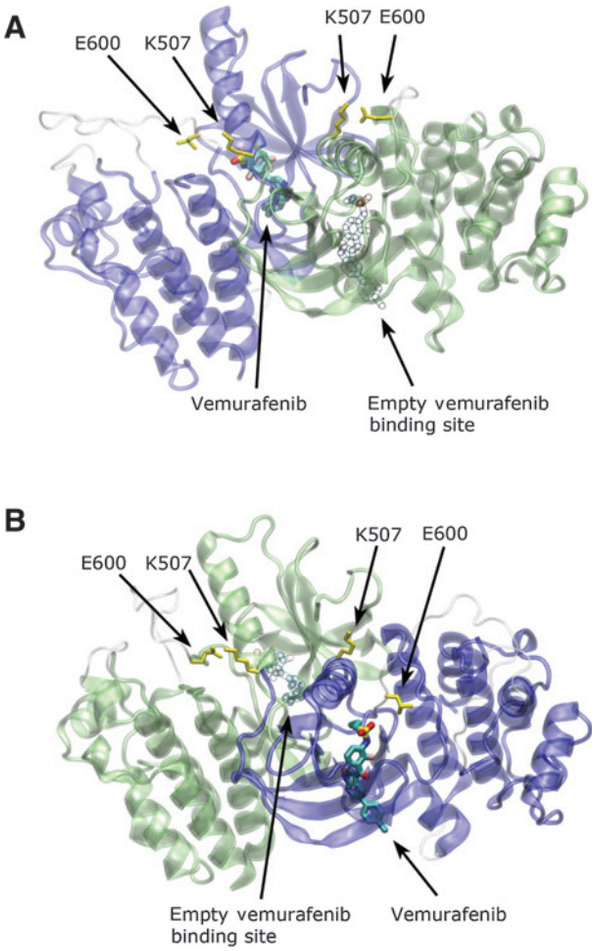

Figure 1.
Three-dimensional representation of the non-crystallographic-symmetry dimer of the kinase domain of BRAF (V600E). A, BRAF bound by vemurafenib is shown in blue and unliganded BRAF in green. The rendering is based on Protein Data Base (PDB; ref. 46) accession code *3OG7* (30). In this structure, several key residues are missing (including E600 of the vemurafenib-liganded B-RAF). These residues were computationally modeled using the FREAD module (47) of MEDELLER (48) and are shown in white. Vemurafenib is colored according to its atom types. For clarity of the orientation, the binding site of vemurafenib in the unliganded BRAF is indicated by a transparent superimposition of vemurafenib. The side–chain interactions between the key residues E600 and K507 for the liganded and unliganded BRAF are highlighted in yellow. B, the identical data as in A are shown with the viewing angle rotated by 180°.

Protein expression pattern

2D gel electrophoresis (2D-PAGE) of the cytoplasmic fraction of A375 and M24met was then performed. Of 750 spots individually cut from the gel, digested and analyzed by nano-LC MS-MS, a total of 588 distinct proteins were successfully identified. In case of 58 spots, no successful identification was achieved, 86 proteins were identified in two different spots, and 18 proteins were identified in three different spots. Three hundred and fifty four of the 588 identified proteins were common or ubiquitously expressed proteins that can be found in a great number of different cell types (23).

Figure 2A and B depicts the high similarity of the protein spot patterns of the melanoma cells (differentially expressed proteins

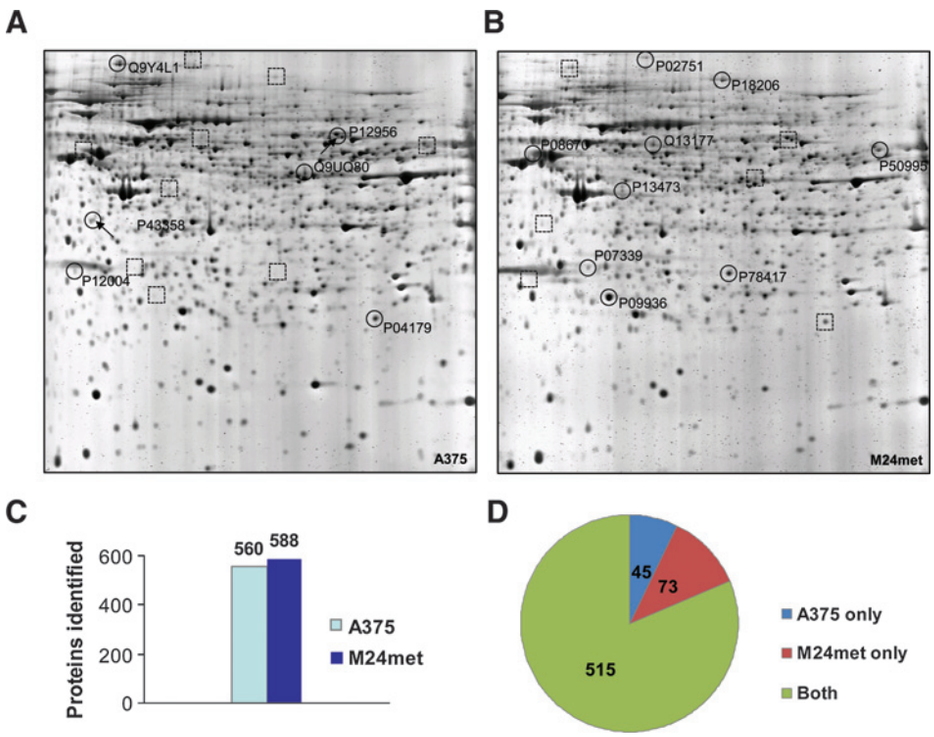

Figure 2.
Proteome characterization of A375 and M24met melanoma cell lines. 2D-gel electrophoresis of A375 (A) and M24met (B). The circle highlights a stronger expression, and the square symbol a weaker expression of the protein, compared with the counterpart. C, comparison of number of proteins identified. D, distribution of proteins identified in both or exclusively expressed in one of these cell lines.

are highlighted). Mass spectrometry of tryptic digests of isolated spots identified 588 different proteins in M24met and 560 proteins in A375 (Fig. 2C); 515 proteins were common to both cell lines (Fig. 2D). All proteins found to be specifically expressed by 2D-PAGE analysis were independently reproduced and verified by shotgun proteomics of the same samples (cytoplasmic fraction of M24met and A375).

Despite their general similarity, we found a different functional signature in the two melanoma cell lines. Proteins found to be upregulated or exclusively expressed in A375 were those involved in differentiation (e.g., P43358: MAGE4:); proliferation (P12004: PCNA or Q9UQ80: proliferation-associated protein 2G4); DNA repair (P12956: 70 kDa subunit of Ku antigen); the p53 pathway and cell cycle (Q13177: serine/threonine-protein kinase PAK2), and redox regulation (P04179: superoxide dismutase or Q9Y4L1: hypoxia-upregulated protein 1; Fig. 2A and B and Supplementary Table S2). In contrast, the M24met cells were found to highly or exclusively overexpress proteins involved in detoxification (P78417: glutathione S-transferase omega-1); metastasis, cell migration and cell motility (P18206: vinculin, P50995: Annexin A11); cell adhesion (P13473: lysosome-associated membrane glycoprotein 2, P18206: vinculin), or EMT (P18206: vinculin, P02751: fibronectin and P08670: vimentin), and lysosomal proteins (P13473: lysosome-associated membrane glycoprotein 2 and P07339: cathepsin D). In addition, a protein involved in the MAPK pathway, P09936: ubiquitin carboxyl-terminal hydrolase isozyme L1 (volume 12.32), was expressed only in M24met (Fig. 2A and B and Supplementary Table S2).

These observations led us to the hypothesis that the upregulated proteins which are the main target of the drug predict the resistance of the melanoma cells, while cells expressing less of these proteins would be sensitive.

Vemurafenib resistance and M8 sensitivity pattern

Recently, we characterized 3,3′,4,4′,5,5′-hexahydroxystilbene (M8), a novel hydroxyl derivative of resveratrol and potent antioxidant, to have superior antitumor activities against melanoma *in vitro* and *in vivo*. M8 was found to act by inhibiting cell proliferation, activating p53, and inducing cell-cycle arrest and DNA damage (13). Because A375 cells overexpress all these features in which M8 interferes, we hypothesized that A375 might be resistant, and vemurafenib-resistant cells sensitive, to M8. Proliferation assay confirmed that indeed, this was the case (Supplementary Table S1).

The vemurafenib-resistant cells V0.5, V1, and V10 were more sensitive to M8 than the sensitive parent cell line V0 (Supplementary Table S1). Subsequently, these cell lines were used to analyze whether the main features such as differential phenotype, differential lysosomal expression, cell adherence features, and EMT are present in a melanoma model with induced vemurafenib resistance. Microscopy revealed that the vemurafenib-sensitive cells V0 exhibited a phenotype of small round cells very similar to the A375 line. Sprouted cells were almost exclusively found in the resistant cell lines commemorating the vemurafenib-resistant M24met (Fig. 3A). Electron microscopy confirmed these findings, also revealing that the vemurafenib-sensitive V0 cells had a ball-like structure and were smaller, whereas the resistant cells were larger and flatter. Similarly, there were fewer and smaller sprouts in the sensitive cells, with the sprouts becoming flatter as vemurafenib resistance increased (Fig. 3B).

Lysosomal staining revealed that the vemurafenib-sensitive V0 cells contained fewer lysosomes and these appeared rather small and granular, whereas in the resistant cell lines, more lysosomes were present and these appeared as larger spherules. In V10, the lysosomes appeared to be excreted and shed by the cells (Fig. 3C).

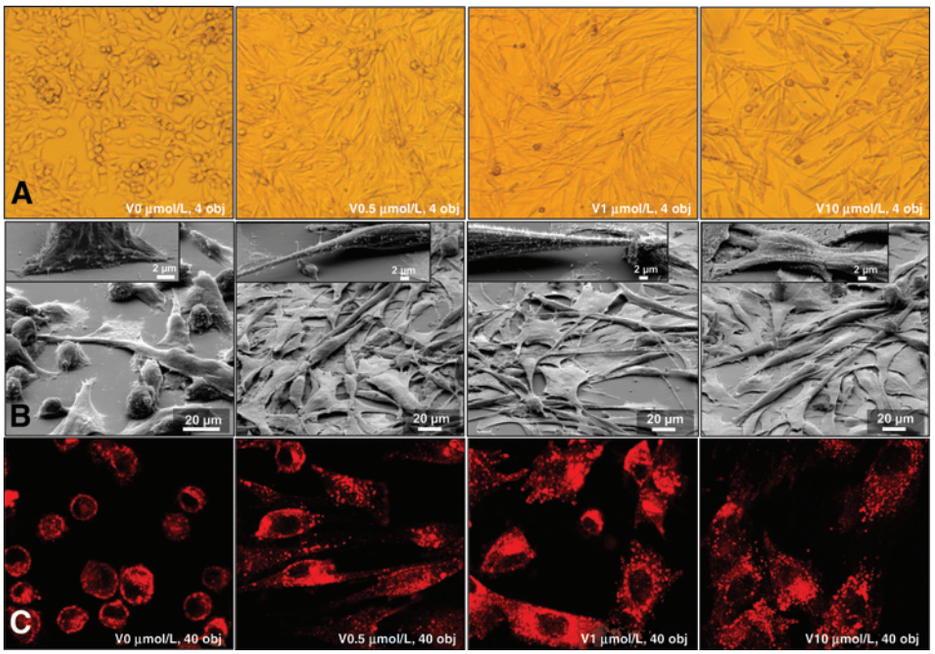

Figure 3.
Microscopic characterization of vemurafenib-sensitive and-resistant melanoma cells V0, V0.5, V1, V10. A, microscopy; B, electron microscopy; C, lysosomal staining.

To verify our observed signature in A375 and M24met melanoma cell lines, we performed shotgun analysis with the well-defined acquired resistance model V0 and V1. Shotgun analysis of the cytoplasmic and nuclear fractions of V0 and V1 was done using QEXACTIVE orbitrap MS. In the cytoplasmic fraction, we identified 5,069 of 48,261 (number of proteins/peptides) in V0 and 4078/34904 in V1. In the nuclear fraction, we identified 4,484 of 41,824 in V0 and 4,029 of 36,322 in V1. Using MaxQuant analysis, we generated heatmaps of the cytoplasmic and nuclear fractions of V0 and V1. Unsupervised hierarchical clustering of Z-scored protein abundances of the cytoplasmic fraction yielded comparable results to the nuclear fraction. The main differences in the cytoplasmic fraction were found in clusters 3 and 4 (Fig. 4), whereas in the nuclear fraction the main differences were in clusters 1 and 5 (Supplementary Fig. S2).

The groups significantly upregulated in V1 were cell adhesion; the lysosomal compartment; cell adhesion molecules; glycosaminoglycan degradation; phagosomes; calcium ion binding; regulation of peptidyl-serine phosphorylation; hydrolase activity; G-protein coupled receptor protein signaling pathway; cell migration; locomotion; chemotaxis; positive regulation of MAPKK cascade, and glycosphingolipid metabolic process. Some of these groups were also found to be upregulated in the nuclear fraction of V1 in addition to, for example, antigen processing and presentation. In comparison, the significant upregulated groups in V0 were different metabolic processes; translational processes; RNA transport and binding; cell cycle processes; NADH dehydrogenase, oxireductase and mitochondrial activity; DNA damage and repair, and signal transduction by p53 (Fig. 4 and Supplementary Fig. S2). Interestingly, the main differences were also detectable by comparing the shotgun data for A375 (comparable with V0) versus M24met (comparable with V1), as presented in Fig. 2 and also reported recently (7). The main differences are summarized in Table 1.

Expression of EMT markers

Because the observed morphologic changes in resistant cells might be due to EMT and EMT markers such as vimentin and fibronectin, shown to be enhanced in the M24met cells (Fig. 5B, Supplementary Table S2), we investigated the different EMT markers. Comparison of shotgun proteome profiles of A375 and M24met was in line with the 2D-gel electrophoresis data. As demonstrated by emPAI values and peptide counts, M24met cells highly expressed mesenchymal proteins such as vimentin, fibronectin, MMP1 (matrix metalloproteinase 1), integrin αV, and ILK-1, whereas A375 exhibited higher expression of the epithelial marker desmoplakin, which is associated with cell adherence (Fig. 5A and B). The most prominent difference was seen in the vimentin expression and this was verified by Western blot analysis (Fig. 5A).

Because EMT is associated with induction of resistance and metastasis (24–26), we performed Western blot analysis of key EMT markers in the vemurafenib-sensitive and -resistant cells. Loss of E-cadherin accompanied by a gain in N-cadherin is considered to be a fundamental event in EMT (25). An E-cadherin/N-cadherin switch was evident in the vemurafenib-resistant cell line, with a total loss of E-cadherin in V0.5 and V1, and low expression of E-cadherin in V10 (Fig. 5C). In the proteome data, we identified only E cadherin in V0, whereas vimentin and further EMT markers such as integrin α and β V were identified with more peptides in V1 (Fig. 5C).

EMT is also associated with a higher expression of MMPs. Zymography Assay confirmed lower expression of MMP-2 in melanocytes than in V0, which in turn showed higher MMP-2 expression than all resistant cell lines. The V0.5 line showed the highest expression of MMPs (Fig. 5D). This is in line with the lower expression of the metalloproteinase inhibitors (TIMPs) 1, 2, and 3 in V1 in comparison with V0 at a peptide level (Fig. 5D).

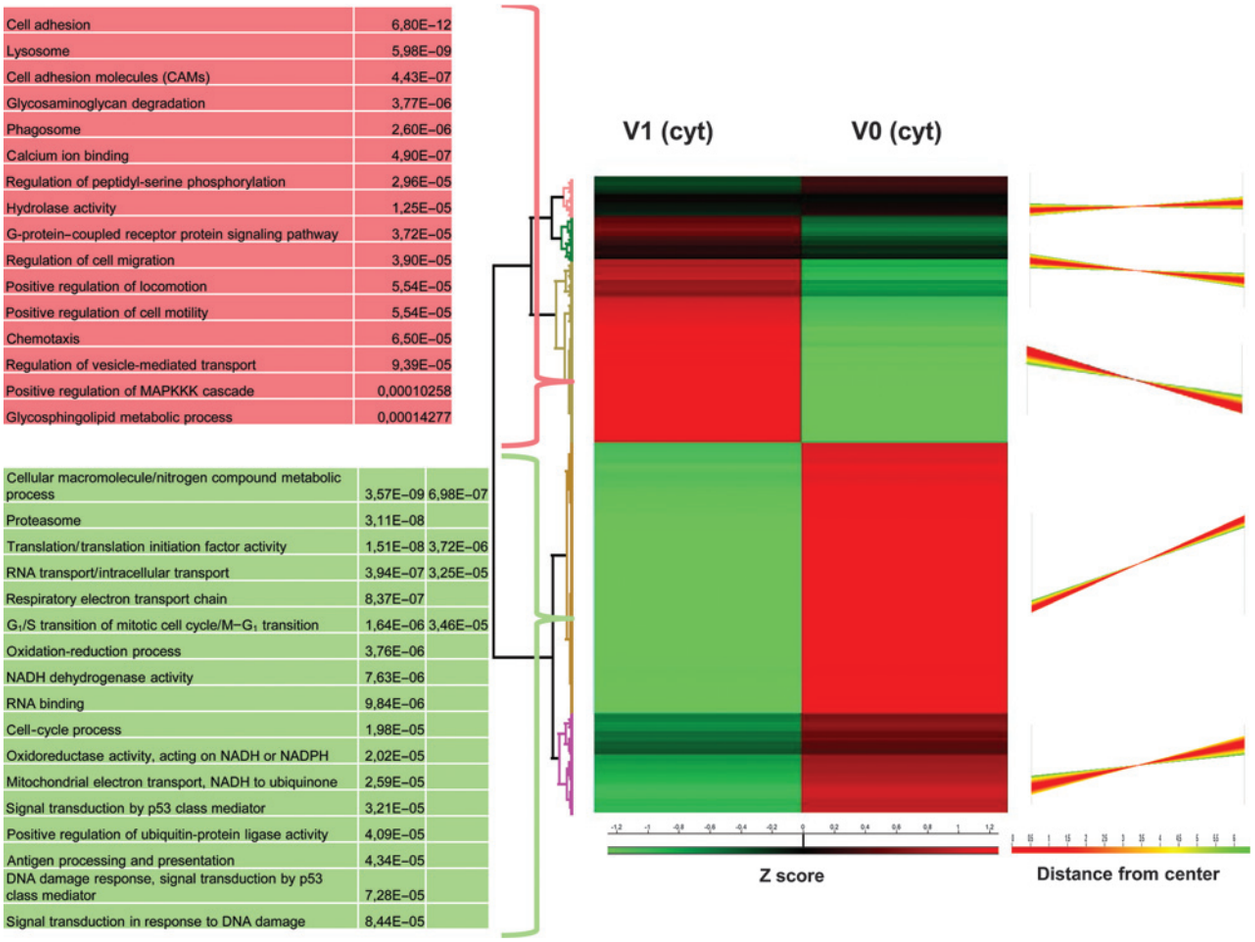

Figure 4.
Proteome characterization of vemurafenib-sensitive and-resistant melanoma cells V0 and V1 (cytoplasmic fraction). Left, hierarchical clustering of Z-scored expression values for significantly changed proteins, revealing differences between V0 and V1. Left, profiles of the five main clusters. Two clusters with the highest difference are selected and the significant regulated groups are depicted. Red, upregulated in V1; green, downregulated in V1.

Adherence to ECM proteins

We previously demonstrated that M24met exhibits a higher capability for cell adherence in contrast with A375 (7). Therefore, we hypothesized that the vemurafenib-resistant cells undergoing EMT have an increased ability to interact with ECM proteins.

A cell adhesion assay (7) confirmed that all vemurafenib-resistant cells adhered with distinctly higher potency to Collagen I. The V0.5 cells adhered to all coated ECM proteins. The highest adherence to collagen IV and laminin I was seen in V0.5, followed by V1 and then V10, whereas the vemurafenib-sensitive V0 cells exhibited no, or marginally measurable, adherence (Fig. 6A and B).

Cell similarity analysis

We subsequently compared the shotgun data of the cytoplasmic fraction of A375 and M24met to those of 226 different cell types and cell states represented in our database, using the Cell Similarity Tool designed by our group (7). A375 was found to have the greatest cell similarity (58%) to melanocytes, whereas M24met exhibited the greatest cell similarity to fibroblasts of multiple myeloma (77%) and endothelial cells stimulated with VEGF (76%; Fig. 6C).

We identified more peptides corresponding to proteins specific for melanocytes in A375 ($n = 24$) compared with M24met ($n = 3$), whereas in M24met, there were more peptides specific for endothelial cells ($n = 14$) compared with A375 ($n = 3$; Fig. 6D).

We identified 995 proteins that were found only in V0 or upregulated 3-fold versus V1; 741 were part of the GPDE, with the highest cell similarity to A375. In contrast, we found 160 proteins exclusive to V1 or upregulated 3-fold versus V0; 99 were part of the GPDE, with the highest cell similarity to fibroblasts of multiple myeloma (Fig. 6C).

Analysis of the number of proteins involved in the gene ontology (GO) annotated inflammatory response did not reveal any difference between A375 ($n = 146$ peptides) and M24met ($n = 147$ peptides). The peptide level correlates with the abundance of the proteins. Nevertheless, A375 showed enhanced expression of peptides specifically involved in inflammation of monocytes, whereas M24met showed enhanced expression of peptides specifically involved in inflammation of fibroblasts

Table 1. Synopsis of vemurafenib resistance signature by comparison of A375/V0 and M24met/V1

Characteristic (method)	A375/V0	M24met/V1
Morphology (H)	Small round cells with smaller cytoplasmic compartment-forming colonies	Sprouted cells with larger cytoplasmic compartment-forming tubes like endothelial cells
Genetic background (PCR, FISH, CGH: data not shown)	A375: NRAS wt; BRAF V600Emut; p16 (CDKN2A) mut; EGFR wt/V0: BRAFV600Emut	M24met: NRAS mut; BRAF wt; p16 (CDKNA2A) deletion; EGFR: amplification/V1: BRAF V600Emut
Similarity (M)	A375: Melanocytes/V0: A375	M24met and V1: fibroblasts (Fib.) of multiple myeloma (MM), V1: Fib. of MM
Sensitivity to vemurafenib (P)	Sensitive	Resistant
Sensitivity to cisplatin (P)	A375: Sensitive	M24met: Resistant
Sensitivity to M8 (P)	Resistant	Sensitive
Cell differentiation (M)	↑	↓
Proliferation, translation (P, M, 2D)	↑	↓
DNA damage/repair capability DNA binding, RNA binding, and transport(M, 2D)	↑	↓
Cell-cycle controlling proteins (M, 2D)	↑	↓
p53 pathway proteins (M, 2D)	↑	↓
Redox homeostasis proteins, oxireductase activity (M)	↑	↓
Mitochondrial activity, NADH dehydrogenase (ubiquinone) activity (M)	↑	↓
Lysosomal compartment, phagosomes, hydrolase activity/glycoshingolipid metabolism (H, M, 2D)	↓	↑
Migration, locomotion, cell motility, chemotaxis, glucosaminoglycan degradation (M, 2D)	↓	↑
Cell adherence/$Ca2^{+}$ ion binding capability/(C, M, 2D)	↓	↑ (M24met: fibrinogen, fibronectin, collagen I/IV; V1: collagen I/IV, laminin)
MAPK pathway proteins (M, 2D)	↓	↑
ECM proteins (WB, H, M, 2D)	↓	↑
EMT markers (WB, M, 2D)	↓	↑
Transformation (M)	Inflammatory proteins of normal fibroblasts	Inflammatory proteins of tumor-associated fibroblasts

Abbreviations: H, histology; CGH, comparative genomic hybridization; M, mass spectrometry; P, proliferation assay; 2D, 2D gel electrophoresis; C, cell adhesion assay; WB, Western blotting; mut, mutated; wt, wild-type; ↑, upregulated; ↓, downregulated.

(Supplementary Fig. S3a). M8 was found to inhibit the inflammatory proteins upregulated in M24met, including lysyl oxidase homolog, plasminogen activator inhibitor 1, ADAMTS-1, pentraxin-related protein (PTX3), and granulins (Supplementary Fig. S3B and S3C). These proteins are all induced by IL1β, while several are induced by VEGF stimulation and/or upregulated in tumor-associated fibroblasts (Supplementary Fig. S3D).

Discussion

Vemurafenib resistance is a key problem for melanoma treatment and an understanding of the underlying mechanisms may help to develop not only predictive and pharmacodynamic biomarkers, but also individualized targeted therapeutic interventions.

Recently, we used proteomics to define the characteristics of cisplatin resistance in melanoma cells (7). Using proteomic methods, we have now extended this profile to further features. The BRAF-mutated A375 is sensitive to both vemurafenib and cisplatin, whereas the NRAS-mutated M24met is resistant. This pattern of sensitivity can be correlated to a distinct morphologic phenotype, genetic background, proteome profile, and cell biology. In addition, we performed proteome analysis of a melanoma model with acquired vemurafenib resistance.

As summarized in Table 1, vemurafenib resistance is characterized by less differentiated and less proliferative cells with expansion of the lysosomal compartment; enhanced expression of proteins involved in the MAPK pathway, metastasis and cell migration, adhesion and ECM proteins, and fewer proteins involved in DNA repair, cell cycle, p53 pathway, and redox homeostasis. Notably, transition from an epidermal to a mesenchymal phenotype was seen, with upregulation of vimentin and fibronectin, a switch from E-cadherin to N-cadherin, higher activity of MMP2, and an enhanced cell adherence function and a melanocytic-endothelial switch.

We predicted that a drug targeting the downregulated proteins might be able to overcome resistance and indeed were able to show that the vemurafenib-resistant cells were highly sensitive to the resveratrol derivative M8. The workflow of the whole study is summarized in Supplementary Fig. S4.

Downregulation of the DNA repair enzyme DNA-dependent protein (DNA-PK) has been linked to a highly aggressive tumor behavior (27). Activation of the DNA-PKC_S results in p53 phosphorylation (28, 29). This observation is in line with our recent findings that M8 induces the phosphorylation of p53, proteins involved in the mismatch repair machinery (MSH6, MSH2, MLH1), and a robust tail moment in a comet assay (13).

Many sophisticated approaches have been investigated in recent times to define vemurafenib resistance. Previous studies demonstrated that the clinical efficacy of a RAF inhibitor requires broad target blockage in BRAF-mutant melanoma (30) and that the MAPK pathway agonist COT drives resistance via MAPK pathway activation (31). Acquired resistance to vemurafenib was linked to mutually exclusive PDGFRβ upregulation or NRAS mutations (8). We found comparable changes in the NRAS-mutated M24met melanoma cell line with an endothelial phenotype.

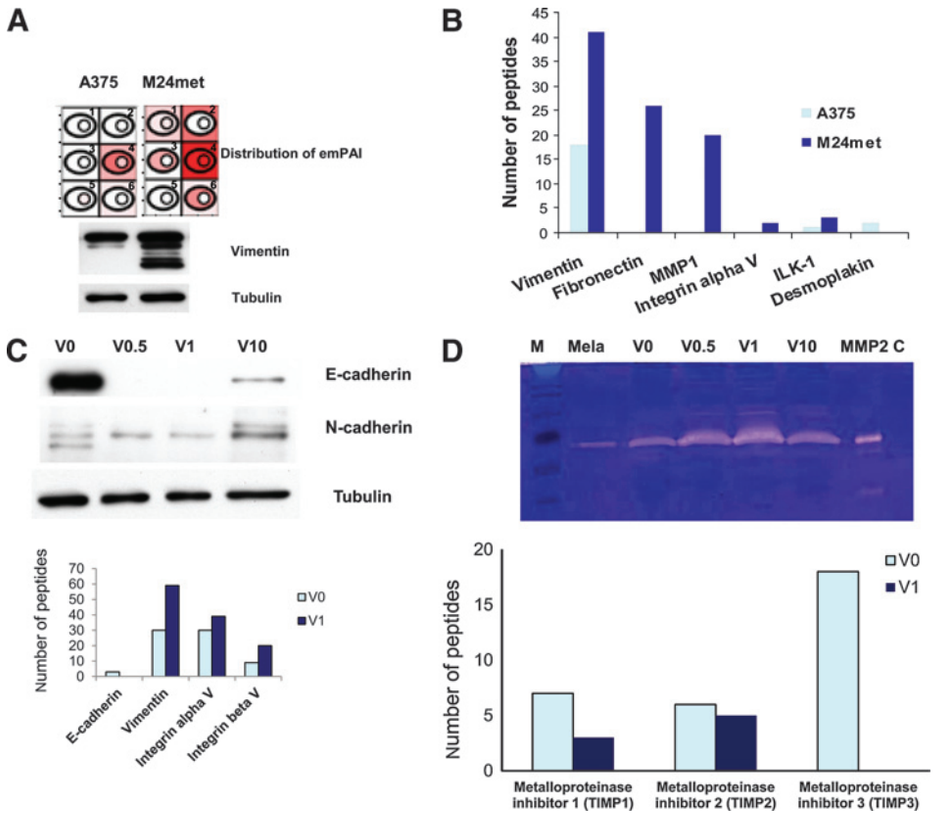

Figure 5.
EMT in A375, M24met melanoma cell lines, and vemurafenib-sensitive and -resistant VM-1 cells. A, distribution of exponentially modified protein abundance index (emPAI) level for [vimentin (1), fibronectin (2), MMP1 (3), integrin α V (4), ILK-1 (5) and desmoplakin (6)] and Western blot analysis of vimentin in A375 and M24met. An increased color intensity of the cell symbol indicates increased emPAI value, as described previously (49). B, distribution of number of peptides in A375 and M24met. C, Western blotting of E-cadherin and N-cadherin in V0, V0.5, V1, and V10; tubulin serves as a positive control and number of peptide level of EMT candidates in V0 and V1. D, zymography assay of melanocytes (mela), V0, V0.5, V1, V10, M (marker) and MMP2 C (MMP2 control) and expression of TIMPs in V0 and V1.

MAPK reactivation was found to predict MEK inhibitor sensitivity (32).

An additional study focused on the influence of the tumor microenvironment on resistance to RAF inhibitors. Proteomic analysis showed that stromal cell secretion of hepatocyte growth factor (HGF) resulted in activation of the HGF receptor MET, with reactivation of MAPK and PI3K–AKT signaling pathways, yielding drug resistance (33).

Until now few proteomic studies have been done to explore vemurafenib resistance. A single study using selected reaction monitoring (SRM) was performed to measure the expression of apoptosis-regulating proteins in the Bcl-2 in melanoma cells with differing PTEN status and vemurafenib resistance/sensitivity (34). In addition, Roesch and colleagues demonstrated, consistent with our preliminary data, that exposure to cisplatin and vemurafenib uniformly leads to enrichment of slow-cycling, long-term tumor-maintaining melanoma cells. Here, proteome profiling identified upregulation of enzymes of mitochondrial oxidative-ATP-synthesis (35). This nicely fits with our observation that the vemurafenib-resistant cells are characterized by a decrease in proliferation, differentiation, and cell-cycle processes but enhanced capability for metastasis and processes of EMT.

Enhanced lysosomal expression, which we demonstrated in the vemurafenib-resistant cells, might improve elimination of the drug from the tumor cell.

The enhancement of the lysosomal compartment and phagosomal processes might be also due to autophagy, which is a multistep process that involves the sequestration of organelles and proteins in autophagic vesicles and subsequent lysosome-dependent degradation (36). Drug-induced autophagy has emerged as a common pathway of resistance to a number of kinase inhibitors, instead less is known about the link between MAPK signaling and autophagy. Very recently, it was demonstrated that BRAFi induces cytoprotective autophagy through activation of an ER stress response and that targeting the ER stress–autophagy pathway might overcome BRAFi resistance in melanoma (36).

Early EMT was shown to be associated with degradation of E-cadherin in the lysosomal compartment and EMT was prevented by lysosomal inhibitors (37). Therefore, vemurafenib resistance might be characterized by lysosomal degradation of E-cadherin and subsequent EMT.

EMT is known to include enhanced cell migration and metastasis, generation of cells with stem cell-like characteristics, and increased resistance to chemotherapy and apoptosis (24–26). E-cadherin loss is a fundamental event, leading to a loss of close cell–cell contact, increased invasiveness and a typical change in morphology (24, 25) and was demonstrated in the vemurafenib-resistant cells. Downregulation or loss of E-cadherin was demonstrated to be sufficient to determine resistance (38, 39) and has been linked to decreased patient survival (40). In parallel to the E-cadherin loss, EMT is involved with induction of the mesenchymal markers N-cadherin, reorganization of the cytoskeleton (switch from cytokeratins to vimentin), and synthesis of ECM proteins and matrix metalloproteases (24, 25, 41). Here, we correlated some of these features with vemurafenib resistance.

Switching to a mesenchymal phenotype increases the ability of a tumor to detach from the epithelial layer and migrate. Enhanced production of ECM proteins and ECM-degrading proteins promotes a more compatible microenvironment and facilitates migration of tumor cells through the host tissue (7).

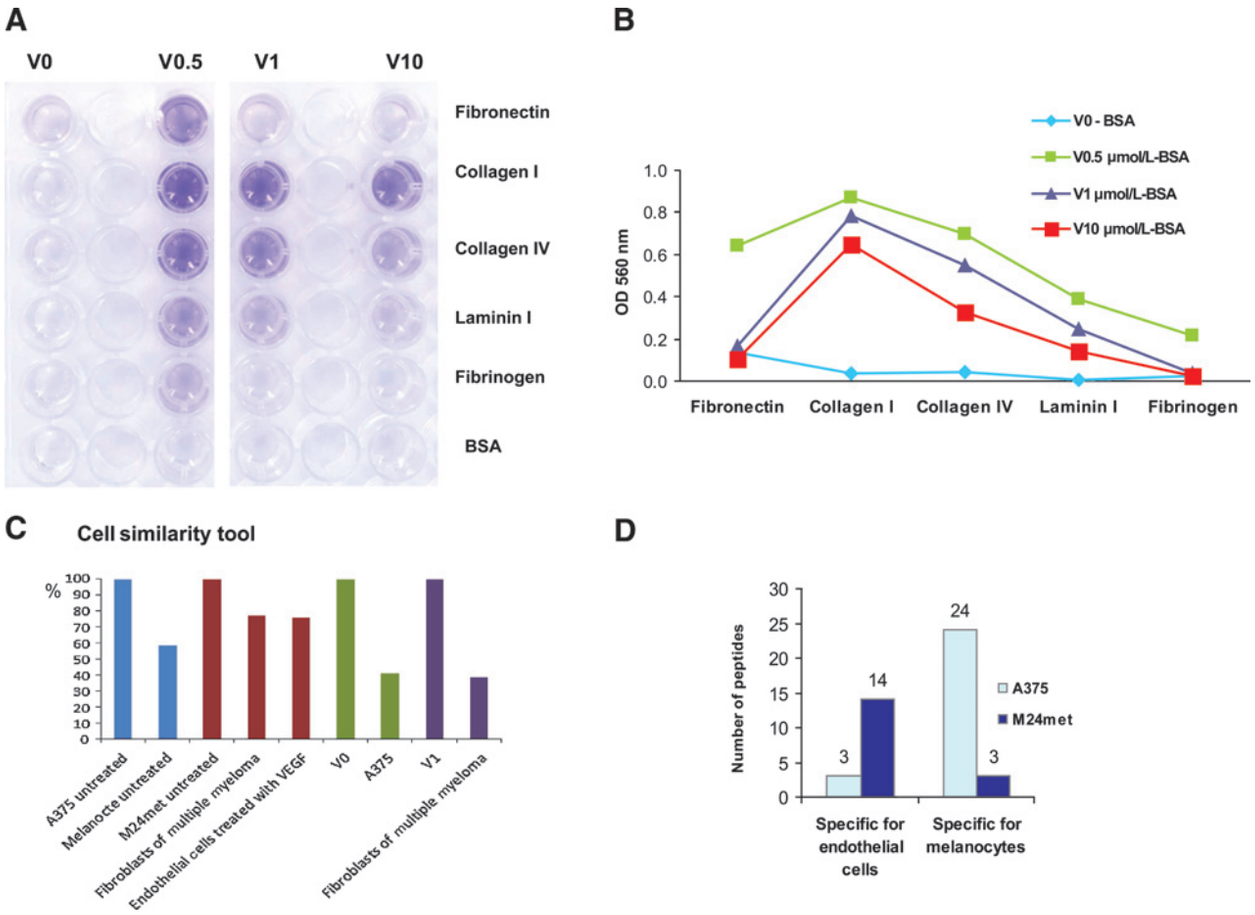

Figure 6.
Differential capability of cell adherence in sensitive and resistant cells. A, cell adhesion assay with V0, V0.5, V1, and V10 (adherent cells stained in an ECM-coated well plate). B, ECM-mediated cell adhesion was quantified at OD 560 nm after extraction. C, comparison of A375, M24met, V0, and V1 with other cells (Cell Similarity Tool). D, expression of proteins specific for endothelial cells and melanocytes in A375 and M24met cells.

Formation of macro-metastases in distant organs is associated with a reversion to an epithelial phenotype (i.e., MET; ref. 25). This reversion was observed at the highest level of induced vemurafenib resistance, as indicated by the cell adhesion assay and reactivation of E-cadherin. It is possible that different molecular mechanisms are involved, depending on the drug concentration used to induce resistance. At lower concentrations, cells might still be able to adapt, while selection of survivors may occur at higher concentrations.

Inflammation has been associated with EMT, especially by COX-2, which induces the expression of Snail1, promoting resistance to anoikis via Ras-MAPK/ERK and PI3K activation (42–45). There was a switch in the profile of inflammatory proteins in M24met, from a normal fibroblast phenotype to a pattern associated with tumor-associated fibroblasts. These secreted peptides (PTX-3, Granulins, and ADAMTS-1) are involved in angiogenesis and/or cell proliferation or adhesion, can be induced in fibroblasts on IL1matrix metalloprotease stimulation, and were found to be regulated by M8. As they can be monitored in blood, they may potentially provide markers for the switch to a resistant phenotype and an indicator for sensitivity to M8.

Thus, applying proteome profiling provides additional insight into mechanisms of tumorigenesis, paving the way for the identification of early biomarkers, development of new drug combinations and individualized patient stratification for optimal therapy using predictive and pharmacodynamic biomarkers. We present seven characteristics which are associated with vemurafenib resistance and might reflect the mode of action of the drug: (i) lysosomal expression, phagosomes, and glycospingolipid process; (ii) metastasis, cell migration, and glycosaminoglycan degradation; (iii) cell adhesion and $Ca2^{+}$ ion-binding capability; (iv) MAPK pathway; (v) enhanced expression of ECM proteins; (vi) EMT; and (vii) enhanced transformation. We also identify seven mechanistic strategies that might help to overcome vemurafenib resistance, namely interfering in (i) cell differentiation; (ii) cell proliferation; (iii) DNA damage/repair; (iv) cell cycle; (v) p53 pathway; (vi) redox homeostasis, and (vii) mitochondrial processes.

We plan to extend these results by evaluating additional sensitive and resistant melanoma cells and melanoma tissue. The proteome analysis will be performed in three steps: (i) Thermo QEXACTIVE will be used for the analysis of cell fractions of vemurafenib-sensitive and -resistant cells. Data will be analyzed

by MaxQuant. (ii) Pressure cycling technology (PCT) SWATH is used for melanoma tissue and offers an optimized protein lysis and extraction by the PCT. Data analysis will be performed by OpenSWATH. (iii) To evaluate the predictive power of markers in blood, SRM is the method of choice. Bioinformatic analysis will be performed by mProphet.

This may offer additional understanding of the underlying mechanisms and new insights for rational therapeutic concepts preventing lethal drug resistance.

Disclosure of Potential Conflicts of Interest

No potential conflicts of interest were disclosed.

Disclaimer

The funders had no role in study design, data collection and analysis, decision to publish, or preparation of the article.

Authors' Contributions

Conception and design: V. Paulitschke, T. Szekeres, H. Pehamberger, C. Gerner, R. Kunstfeld

Development of methodology: V. Paulitschke, W. Berger, P. Paulitschke, T. Szekeres, A. Meshcheryakova, C. Pirker, C. Gerner

Acquisition of data (provided animals, acquired and managed patients, provided facilities, etc.): V. Paulitschke, E. Hofstaetter, R. Dingelmaier-Hovorka, D. Födinger, W. Jäger, A. Meshcheryakova, A. Bileck, C. Gerner

Analysis and interpretation of data (e.g., statistical analysis, biostatistics, computational analysis): V. Paulitschke, W. Berger, E. Hofstaetter, B. Knapp, A. Meshcheryakova, A. Bileck, C. Gerner

Writing, review, and/or revision of the manuscript: V. Paulitschke, W. Berger, P. Paulitschke, B. Knapp, W. Jäger, A. Meshcheryakova, C. Pirker, H. Pehamberger, R. Kunstfeld

Administrative, technical, or material support (i.e., reporting or organizing data, constructing databases): V. Paulitschke, B. Knapp, R. Dingelmaier-Hovorka, D. Födinger, C. Gerner, R. Kunstfeld

Study supervision: V. Paulitschke, R. Kunstfeld

Acknowledgments

The authors thank Julia Balfour (Dundee, Scotland) for editorial assistance, Rosa-Maria Weiss for establishing the vemurafenib-resistant VM-1 cells, and Johannes Griss M.D., Ph.D. for bioinformatic assistance.

Grant Support

This work was supported by the following grants of the "Austrian Federal Reserve Bank": Project No. 12215 (to V. Paulitschke) and No. 11425 (to R. Kunstfeld), No. 12747 (to A.B. Riemer and R. Kunstfeld), the "Interdisziplinärer Krebsforschungsfond" (to V. Paulitschke), "Hans und Blanca Moser Stipendium" (to V. Paulitschke), and "Medical Scientific Fund of the Mayor of the City of Vienna" (to V. Paulitschke).

The costs of publication of this article were defrayed in part by the payment of page charges. This article must therefore be hereby marked *advertisement* in accordance with 18 U.S.C. Section 1734 solely to indicate this fact.

Received August 19, 2014; revised December 22, 2014; accepted January 8, 2015; published OnlineFirst January 22, 2015.

References

1. Markovic SN, Erickson LA, Rao RD, Weenig RH, Pockaj BA, Bardia A, et al. Malignant melanoma in the 21st century, part 2: staging, prognosis, and treatment. Mayo Clin Proc 2007;82:490–513.
2. Bhatia S, Thompson JA. Systemic therapy for metastatic melanoma in 2012: dawn of a new era. J Natl Compr Canc Netw 2012;10:403–12.
3. Hodi FS, O'Day SJ, McDermott DF, Weber RW, Sosman JA, Haanen JB, et al. Improved survival with ipilimumab in patients with metastatic melanoma. N Engl J Med 2010;363:711–23.
4. Chapman PB, Hauschild A, Robert C, Haanen JB, Ascierto P, Larkin J, et al. Improved Survival with Vemurafenib in Melanoma with BRAF V600E Mutation. N Engl J Med 2011;364:2507–16.
5. Wagle N, Emery C, Berger MF, Davis MJ, Sawyer A, Pochanard P, et al. Dissecting therapeutic resistance to RAF inhibition in melanoma by tumor genomic profiling. J Clin Oncol 2011;29:3085–96.
6. Dummer R, Flaherty KT. Resistance patterns with tyrosine kinase inhibitors in melanoma: new insights. Curr Opin Oncol 2012;24:150–4.
7. Paulitschke V, Haudek-Prinz V, Griss J, Berger W, Mohr T, Pehamberger H, et al. Functional classification of cellular proteome profiles support the identification of drug resistance signatures in melanoma cells. J Proteome Res 2013;12:3264–76.
8. Nazarian R, Shi H, Wang Q, Kong X, Koya RC, Lee H, et al. Melanomas acquire resistance to B-RAF(V600E) inhibition by RTK or N-RAS upregulation. Nature 2010;468:973–7.
9. Trunzer K, Pavlick AC, Schuchter L, Gonzalez R, McArthur GA, Hutson TE, et al. Pharmacodynamic effects and mechanisms of resistance to vemurafenib in patients with metastatic melanoma. J Clin Oncol 2013;31:1767–74.
10. Paulitschke V, Gruber S, Hofstatter E, Haudek-Prinz V, Klepeisz P, Schicher N, et al. Proteome analysis identified the PPARgamma ligand 15d-PGJ2 as a novel drug inhibiting melanoma progression and interfering with tumor-stroma interaction. PLoS ONE 2012;7:e46103.
11. Heffeter P, Atil B, Kryeziu K, Groza D, Koellensperger G, Korner W, et al. The ruthenium compound KP1339 potentiates the anticancer activity of sorafenib *in vitro* and *in vivo*. Eur J Cancer 2013;49:3366–75.
12. Mathieu V, Pirker C, Schmidt WM, Spiegl-Kreinecker S, Lotsch D, Heffeter P, et al. Aggressiveness of human melanoma xenograft models is promoted by aneuploidy-driven gene expression deregulation. Oncotarget 2012;3:399–413.
13. Paulitschke V, Schicher N, Szekeres T, Jager W, Elbling L, Riemer AB, et al. 3,3′,4,4′,5,5′-hexahydroxystilbene impairs melanoma progression in a metastatic mouse model. J Invest Dermatol 2010;130:1668–79.
14. Slany A, Haudek-Prinz V, Meshcheryakova A, Bileck A, Lamm W, Zielinski C, et al. Extracellular matrix remodeling by bone marrow fibroblast-like cells correlates with disease progression in multiple myeloma. J Proteome Res 2014;13:844–54.
15. Bray DF, Bagu J, Koegler P. Comparison of hexamethyldisilazane (HMDS), Peldri II, and critical-point drying methods for scanning electron microscopy of biological specimens. Microsc Res Tech 1993;26:489–95.
16. Hoeller C, Thallinger C, Pratscher B, Bister MD, Schicher N, Loewe R, et al. The non-receptor-associated tyrosine kinase Syk is a regulator of metastatic behavior in human melanoma cells. J Invest Dermatol 2005;124:1293–9.
17. Slany A, Haudek-Prinz V, Zwickl H, Stattner S, Grasl-Kraupp B, Gerner C. Myofibroblasts are important contributors to human hepatocellular carcinoma: evidence for tumor promotion by proteome profiling. Electrophoresis 2013;34:3315–25.
18. Rabilloud T, Strub JM, Luche S, van Dorsselaer A, Lunardi J. A comparison between Sypro Ruby and ruthenium II tris (bathophenanthroline disulfonate) as fluorescent stains for protein detection in gels. Proteomics 2001;1:699–704.
19. Bileck A, Kreutz D, Muqaku B, Slany A, Gerner C. Comprehensive assessment of proteins regulated by dexamethasone reveals novel effects in primary human peripheral blood mononuclear cells. J Proteome Res 2014;13:5989–6000.
20. Cox J, Mann M. MaxQuant enables high peptide identification rates, individualized p.p.b.-range mass accuracies and proteome-wide protein quantification. Nat Biotechnol 2008;26:1367–72.
21. Cox J, Mann M. 1D and 2D annotation enrichment: a statistical method integrating quantitative proteomics with complementary high-throughput data. BMC Bioinformatics 2012;13 Suppl 16:S12.
22. Geiger T, Cox J, Mann M. Proteomic changes resulting from gene copy number variations in cancer cells. PLoS Genet 2010;6:e1001090.

23. Slany A, Haudek VJ, Gundacker NC, Griss J, Mohr T, Wimmer H, et al. Introducing a new parameter for quality control of proteome profiles: consideration of commonly expressed proteins. Electrophoresis 2009;30: 1306–28.
24. Thiery JP, Acloque H, Huang RY, Nieto MA. Epithelial-mesenchymal transitions in development and disease. Cell 2009;139:871–90.
25. Kalluri R, Weinberg RA. The basics of epithelial-mesenchymal transition. J Clin Invest 2009;119:1420–8.
26. Gao D, Vahdat LT, Wong S, Chang JC, Mittal V. Microenvironmental regulation of epithelial-mesenchymal transitions in cancer. Cancer Res 2012;72:4883–9.
27. Korabiowska M, Quentin T, Schlott T, Bauer H, Kunze E. Down-regulation of Ku 70 and Ku 80 mRNA expression in transitional cell carcinomas of the urinary bladder related to tumor progression. World J Urol 2004; 22:431–40.
28. Shieh SY, Ikeda M, Taya Y, Prives C. DNA damage-induced phosphorylation of p53 alleviates inhibition by MDM2. Cell 1997;91:325–34.
29. Tibbetts RS, Brumbaugh KM, Williams JM, Sarkaria JN, Cliby WA, Shieh SY, et al. A role for ATR in the DNA damage-induced phosphorylation of p53. Genes Dev 1999;13:152–7.
30. Bollag G, Hirth P, Tsai J, Zhang J, Ibrahim PN, Cho H, et al. Clinical efficacy of a RAF inhibitor needs broad target blockade in BRAF-mutant melanoma. Nature 2010;467:596–9.
31. Johannessen CM, Boehm JS, Kim SY, Thomas SR, Wardwell L, Johnson LA, et al. COT drives resistance to RAF inhibition through MAP kinase pathway reactivation. Nature 2010;468:968–72.
32. Poulikakos PI, Persaud Y, Janakiraman M, Kong X, Ng C, Moriceau G, et al. RAF inhibitor resistance is mediated by dimerization of aberrantly spliced BRAF(V600E). Nature 2011;480:387–90.
33. Straussman R, Morikawa T, Shee K, Barzily-Rokni M, Qian ZR, Du J, et al. Tumour micro-environment elicits innate resistance to RAF inhibitors through HGF secretion. Nature 2012;487:500–4.
34. Koomen JM, Smalley KS. Using quantitative proteomic analysis to understand genotype specific intrinsic drug resistance in melanoma. Oncotarget 2011;2:329–35.
35. Roesch A, Vultur A, Bogeski I, Wang H, Zimmermann KM, Speicher D, et al. Overcoming intrinsic multidrug resistance in melanoma by blocking the mitochondrial respiratory chain of slow-cycling JARID1B(high) cells. Cancer Cell 2013;23:811–25.
36. Ma XH, Piao SF, Dey S, McAfee Q, Karakousis G, Villanueva J, et al. Targeting ER stress-induced autophagy overcomes BRAF inhibitor resistance in melanoma. J Clin Invest 2014;124:1406–17.
37. Janda E, Nevolo M, Lehmann K, Downward J, Beug H, Grieco M. Raf plus TGFbeta-dependent EMT is initiated by endocytosis and lysosomal degradation of E-cadherin. Oncogene 2006;25:7117–30.
38. Onder TT, Gupta PB, Mani SA, Yang J, Lander ES, Weinberg RA. Loss of E-cadherin promotes metastasis via multiple downstream transcriptional pathways. Cancer Res 2008;68:3645–54.
39. Derksen PW, Liu X, Saridin F, van der Gulden H, Zevenhoven J, Evers B, et al. Somatic inactivation of E-cadherin and p53 in mice leads to metastatic lobular mammary carcinoma through induction of anoikis resistance and angiogenesis. Cancer Cell 2006;10:437–49.
40. Hirohashi S. Inactivation of the E-cadherin-mediated cell adhesion system in human cancers. Am J Pathol 1998;153:333–9.
41. Sanchez-Tillo E, Liu Y, de Barrios O, Siles L, Fanlo L, Cuatrecasas M, et al. EMT-activating transcription factors in cancer: beyond EMT and tumor invasiveness. Cell Mol Life Sci 2012;69:3429–56.
42. Dohadwala M, Yang SC, Luo J, Sharma S, Batra RK, Huang M, et al. Cyclooxygenase-2-dependent regulation of E-cadherin: prostaglandin E (2) induces transcriptional repressors ZEB1 and snail in non-small cell lung cancer. Cancer Res 2006;66:5338–45.
43. Vega S, Morales AV, Ocana OH, Valdes F, Fabregat I, Nieto MA. Snail blocks the cell cycle and confers resistance to cell death. Genes Dev 2004;18:1131–43.
44. Neil JR, Johnson KM, Nemenoff RA, Schiemann WP. Cox-2 inactivates Smad signaling and enhances EMT stimulated by TGF-beta through a PGE2-dependent mechanisms. Carcinogenesis 2008;29: 2227–35.
45. Greenhough A, Smartt HJ, Moore AE, Roberts HR, Williams AC, Paraskeva C, et al. The COX-2/PGE2 pathway: key roles in the hallmarks of cancer and adaptation to the tumour microenvironment. Carcinogenesis 2009;30: 377–86.
46. Berman HM, Westbrook J, Feng Z, Gilliland G, Bhat TN, Weissig H, et al. The protein data bank. Nucleic Acids Res 2000;28:235–42.
47. Choi Y, Deane CM. FREAD revisited: Accurate loop structure prediction using a database search algorithm. Proteins 2010;78:1431–40.
48. Kelm S, Shi J, Deane CM. MEDELLER: homology-based coordinate generation for membrane proteins. Bioinformatics 2010;26: 2833–40.
49. Ishihama Y, Oda Y, Tabata T, Sato T, Nagasu T, Rappsilber J, et al. Exponentially modified protein abundance index (emPAI) for estimation of absolute protein amount in proteomics by the number of sequenced peptides per protein. Mol Cell Proteomics 2005;4: 1265–72.